Supporting Information

Graphitization Induced by KOH Etching for the Fabrication of Hierarchical Porous Graphitic Carbon Sheets for High Performance Supercapacitors

Fulai Qi, [a,b] *Zhangxun Xia,* [a] *Ruili Sun,* [a,b] *Xuejing Sun,* [a,b] *Xinlong Xu,* [a,b] *Wei Wei,* [a] *Suli Wang,* [a*] *and Gongquan Sun* [a]*

[a] Dalian National Laboratory for Clean Energy, Dalian Institute of Chemical Physics, Chinese Academy of Sciences, Dalian 116023, China

E-mail: suliwang@dicp.ac.cn

E-mail: gqsun@dicp.ac.cn

[b] University of Chinese Academy of Sciences, Beijing 100039, China

Keywords: graphitic carbon nanosheet; hierarchical pore; high surface area; KOH etching; energy shorage

Characterizations and instruments:

The microstructure was observed by Field emission scanning electron microscopy (FE-SEM, JSM-7800F). Transmission electron microscopy (TEM) was carried out on a JEM-2100F instrument (JEOL). The samples for TEM analysis were prepared by adding a few drops of colloidal suspension onto a hollow copper grid and drying under infrared light.

The surface area and pore size distributions were determined from the N_2 adsorption isotherms at 77.4 K using an Autosorb iQ2 instrument. Before analysis, the samples were out-gassed at 300 °C under vacuum for 3 h. The specific surface areas were calculated using adsorption data by the Multi-Point Brunauer-Emmett-Teller (BET) method. Pore size distribution (PSD) curves were computed using the nonlocal hybrid density functional theory (NLDFT) method assuming slit/cylindrical pore geometry for the micropores and a cylindrical pore geometry for the mesopores.

The N/P functional groups on the HPGCS surface were analyzed with a Fourier transform infrared (FT-IR) spectrometer (Nicolet 6700) in the absorbance mode (4000-500 cm^{-1}; number of scans: 64; resolution: 2 cm^{-1}). Samples for FTIR measurements were prepared by pressing the mixture (powders of HMCAs and KBr powders) into a tablet.

X-ray photoelectron spectroscopy (XPS) measurements were carried out using an ultrahigh vacuum setup equipped with a KAlpha electron spectrometer (Thermo Fisher) with an Al Ka X-ray source (excitation energy of 1486.71 eV). All the binding energies were determined relative to the C1s XPS peak at 284.6 eV. And XPS PEAK

Version 4.1 was used to fit the narrow scan spectra of N1s and P2p after Shirley type background subtraction.

The crystallographic characterization of the as-synthesized HPGCS was obtained on an X'pert Pro diffractometer with monochromated Cu-Kα radiation (40 kV, 200 mA) at a scan rate of 5° per minute. Raman spectras were recorded using an inVia Raman microscope with 532 nm incident radiation. The Raman shift was calibrated by the G-band position of HOPG (1582 cm^{-1}), and the intensity was normalized by the G-band.

Electrochemical performance of HPGCS: The electrochemical characteristics of HPGCS were evaluated with cyclic voltammetry (CV), galvanostatic charge/discharge (GCD) (CHI 760E electrochemical workstation, CHInstruments). The frequency response was analyzed by electrochemical impedance spectroscopy (EIS) (Solartron SI1260 and Solartron SI1287) in a frequency range of 0.1 Hz to 100 kHz with a 10 mV voltage amplitude.The working electrode was prepared by mixing 80 wt% of as-obtained carbon, 10 wt% of acetylene black, and 10 wt% of PTFE binder in ethanol. The mixture was grinded into a paste using a mortar and pestle, rolled into uniform thickness sheets and punched into ~1cm diameter electrodes. A pair of typical electrodes had a weight ca. 2 mg after drying overnight at a ~ 100 °C under vacuum. After drying, the electrode was pressured on stainless steel mesh current collector under 10 MPa for 30 s. The two identical (by weight and size) electrodes were assembled in a 2032 test cell, which consisted of two current collectors, two electrodes, and an ion-porous separator (Celgard® 3501). The

electrolyte solution was 1M tetraethylammonium tetrafluoroborate ($TEABF_4$) in acetonitrile (AN) solution for organic cells. The assembly of the test cell was done in a glove box filled with Ar.

The C_S of electrode in two-electrode system was calculated from GCD using the following equation:

$$C_S=2I/(m\Delta V/\Delta t)$$

where I, m, and $\Delta V/\Delta t$ are the applied current density, the mass of the active material mass for a single electrode (g), and the discharge slope, respectively. The specific energy (E_{cell}) and specific power (P_{cell}) for symmetrical supercapacitors were also calculated by using equations:

$$E_{cell}= C_S\Delta V^2/(8\times3.6)$$

$$P_{cell}= E_{cell}/t$$

Where ΔV (V) is the cell potential including iR drop and t is discharge time (After unit conversion including gram into kilogram, second into hour, the coefficient in the formula of E_{cell} will be added).

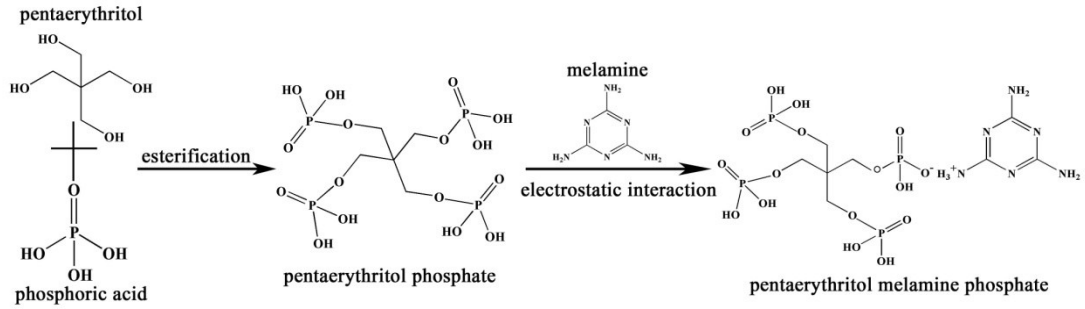

Fig. S1 The synthesis process of PMP precursor. A simple esterification of phosphoric acid and pentaerythritol was carried out to obtain pentaerythritol phosphate, followed by neutralization reaction with melamine

Fig. S2 The optical photo of the foam-like architecture from PMP precursor after thermal annealing at 500 ºC for 2 hours.

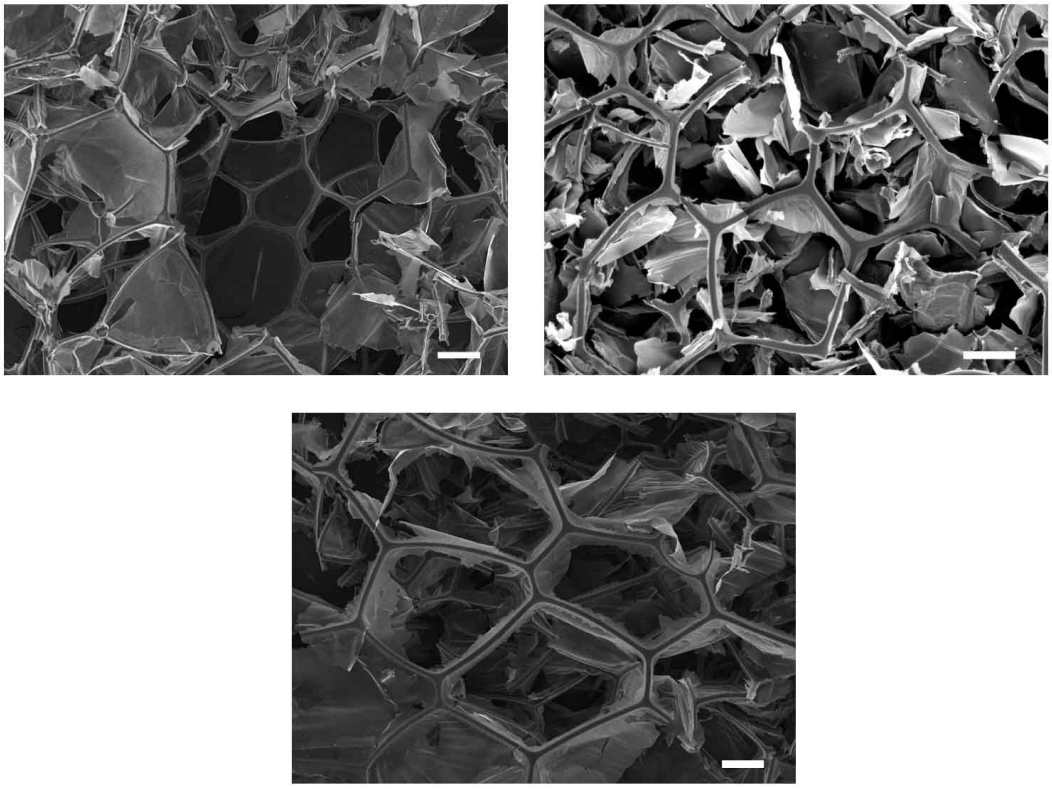

Fig. S3 The SEM images of the MS-x (600, 700, 800). Scale bar is 50 μm.

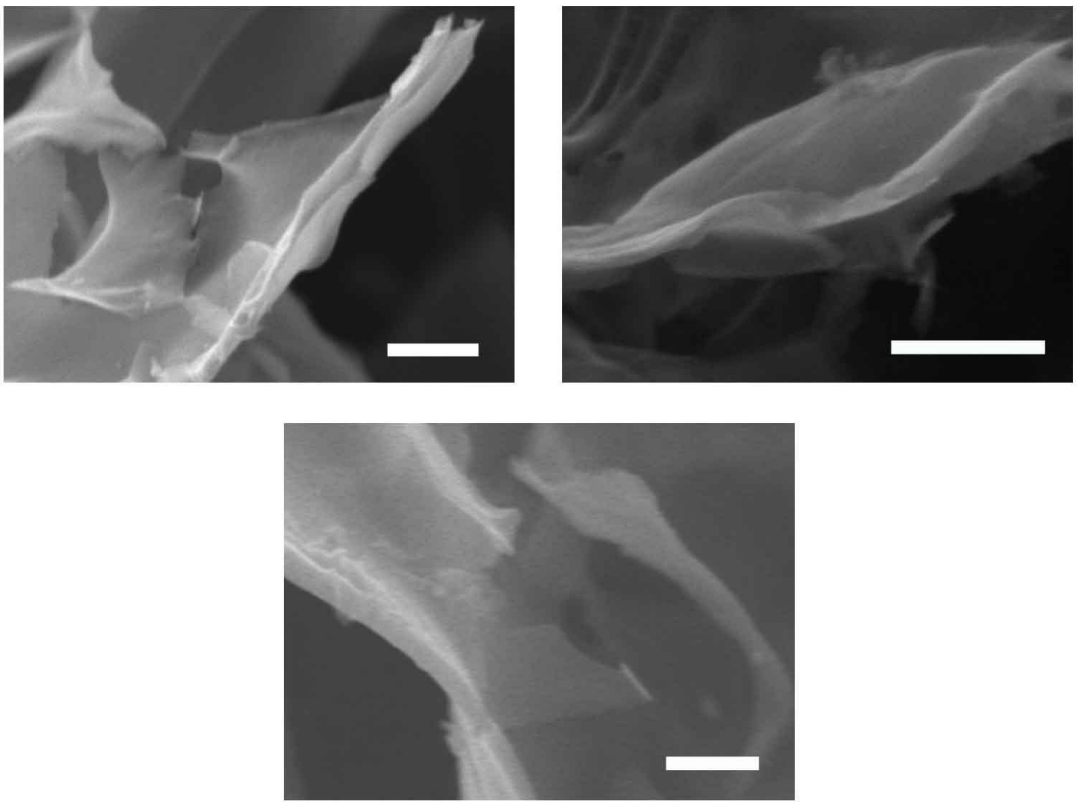

Fig. S4 The TEM images of the HPGCS-x (500, 700, 800). Scale bar is 200 nm.

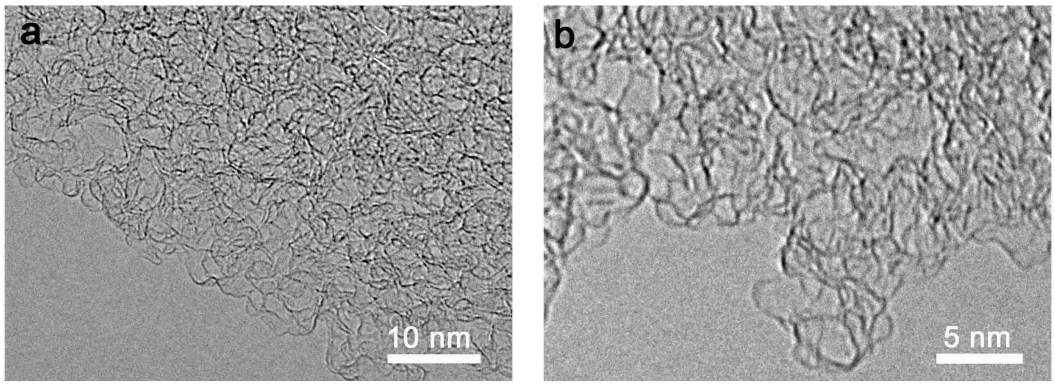

Fig. S5 The TEM images with different magnifications of the HPGCS-600

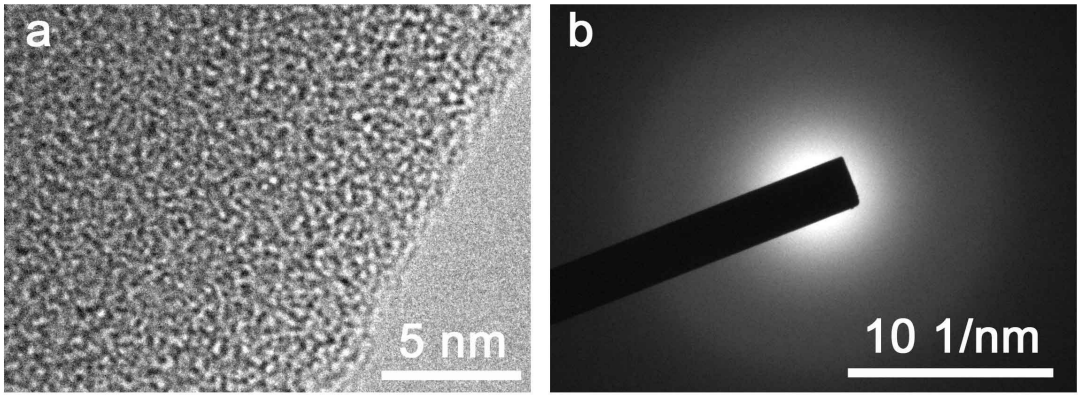

Fig. S6 Structure and morphology of MS-600. (a) HR-TEM image of MS-600, (b) SAED image of MS-600.

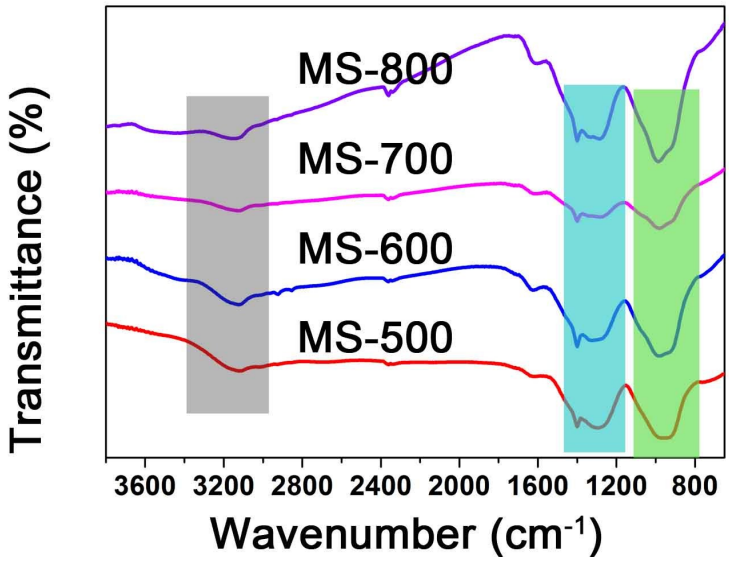

Fig. S7 The FTIR spectra of MS-x.

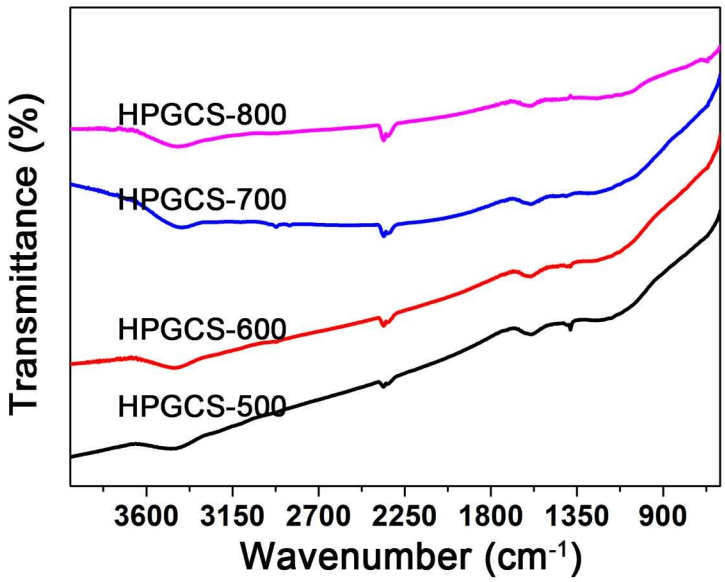

Fig. S8 The FTIR spectra of HPGCS-x.

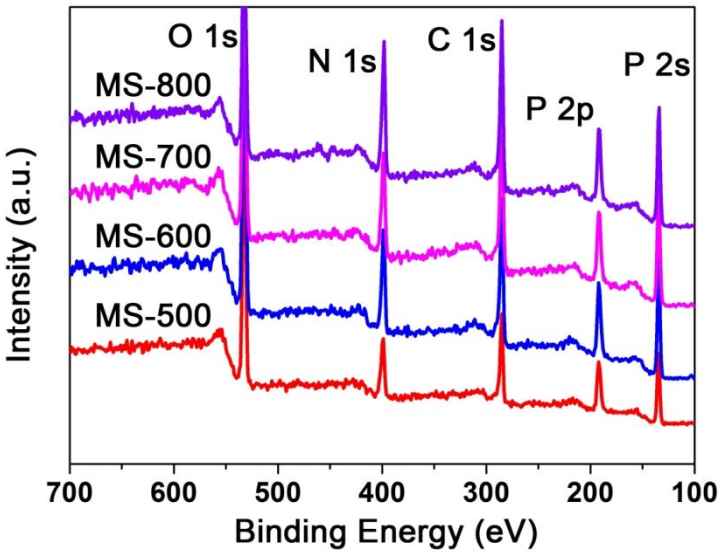

Fig. S9 The XPS survey spectra of MS-x.

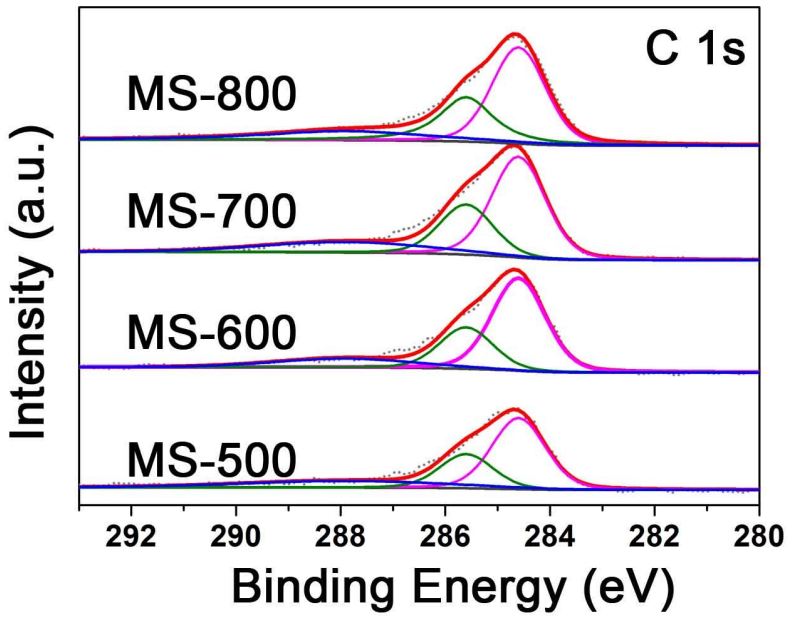

Fig. S10 The high-resolution XPS C 1s spectra of MS-x.[1]

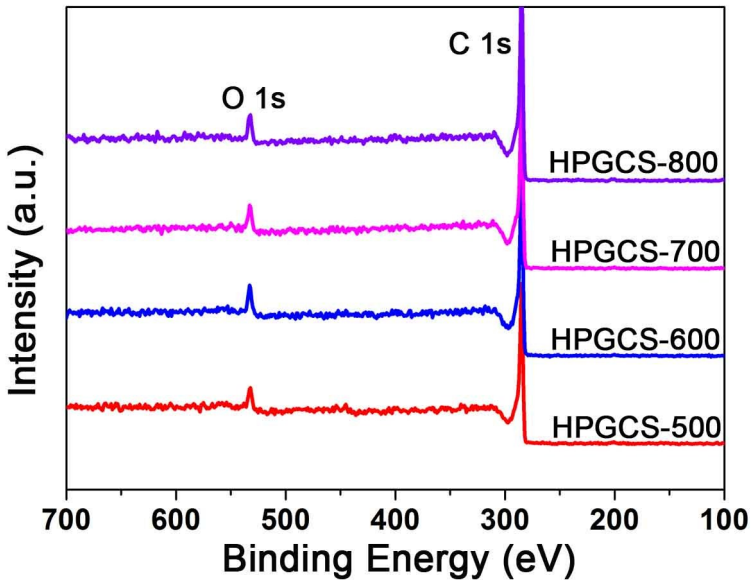

Fig. S11 The XPS survey spectra of HPGCS-x.

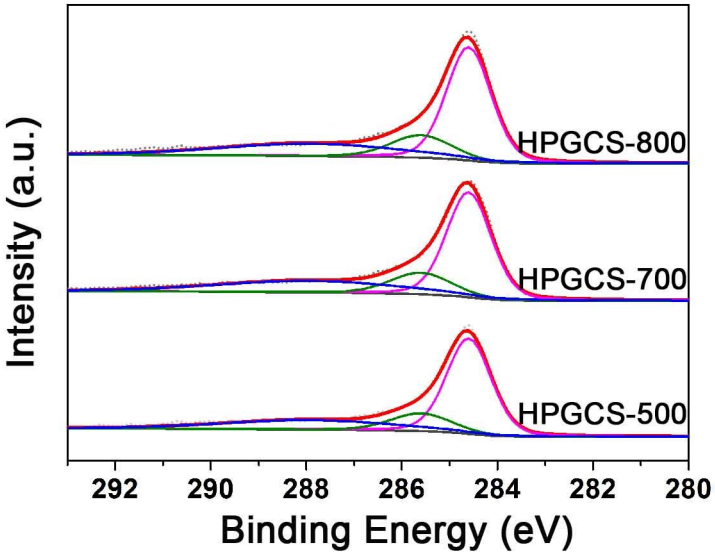

Fig. S12 The high-resolution XPS C 1s spectra of HPGCS-x.[1]

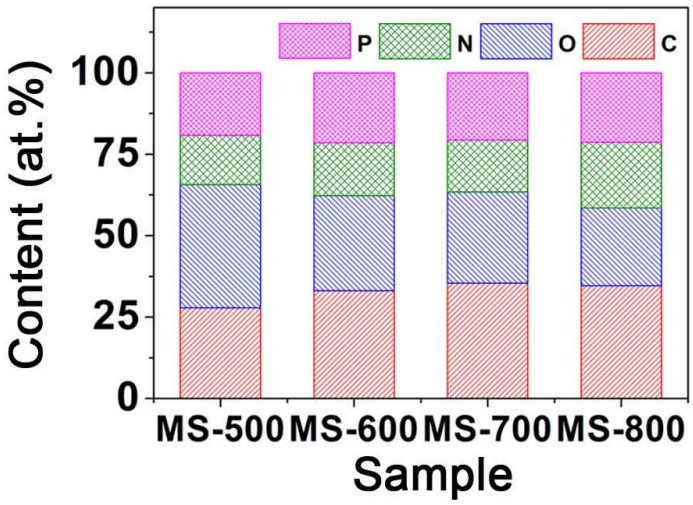

Fig. S13 The percentage content of C, O, N, P from XPS survey spectra of MS-x.

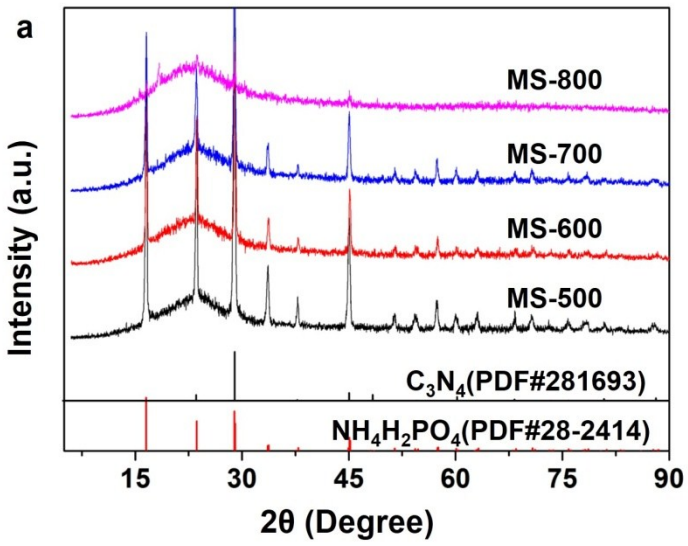

Fig. 14 XRD patterns of MS-x

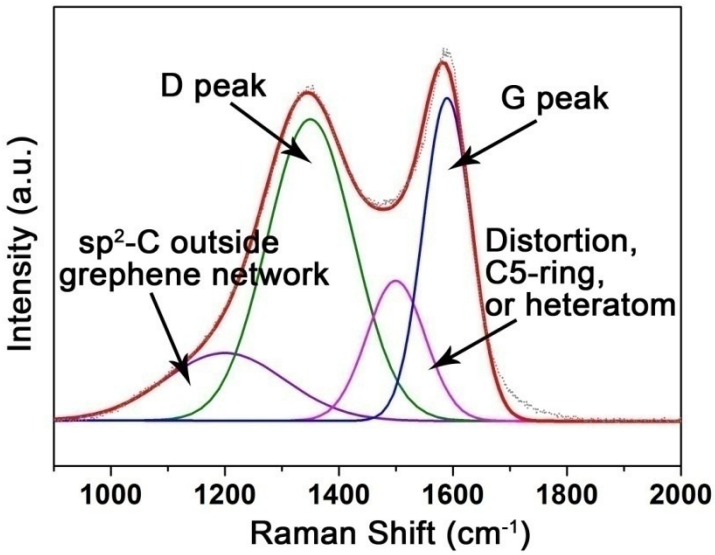

Fig. S15 The Raman spectroscopy of of HPGCS-x with four fitted Lorentzian peaks.[2]

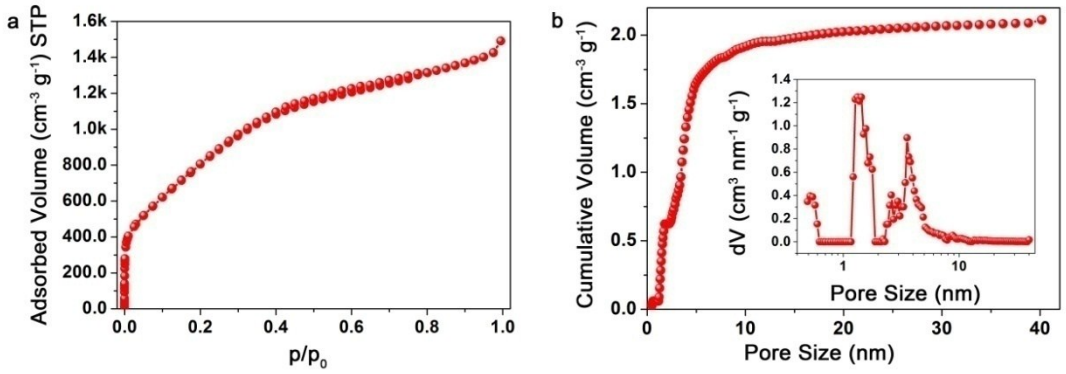

Fig. 16 (a) Nitrogen adsorption/desorption isotherms of HPGCS-500. (b) Cumulative pore volume and pore size distribution (inset) from N_2 adsorption for HPGCS.

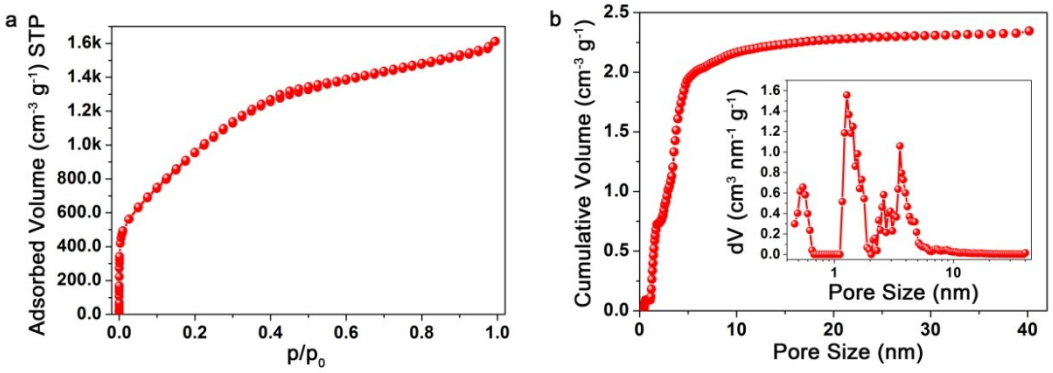

Fig. 17 (a) Nitrogen adsorption/desorption isotherms of HPGCS-700. (b) Cumulative pore volume and pore size distribution (inset) from N_2 adsorption for HPGCS.

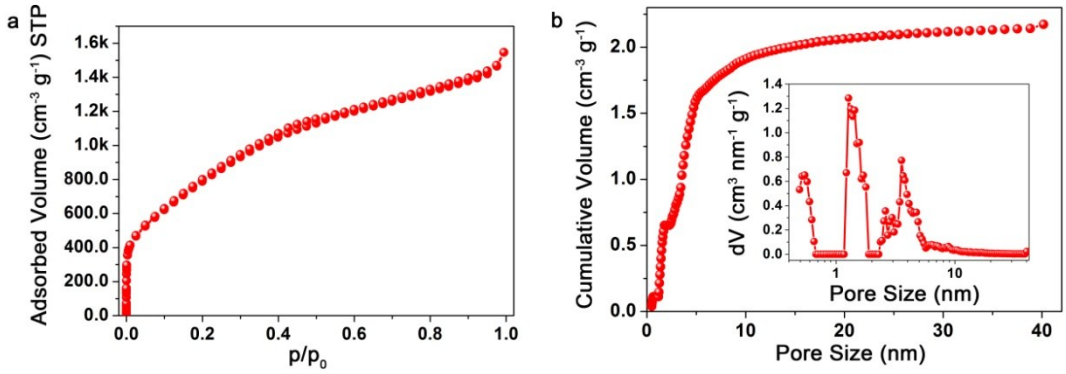

Fig. 18 (a) Nitrogen adsorption/desorption isotherms of HPGCS-800. (b) Cumulative pore volume and pore size distribution (inset) from N_2 adsorption for HPGCS.

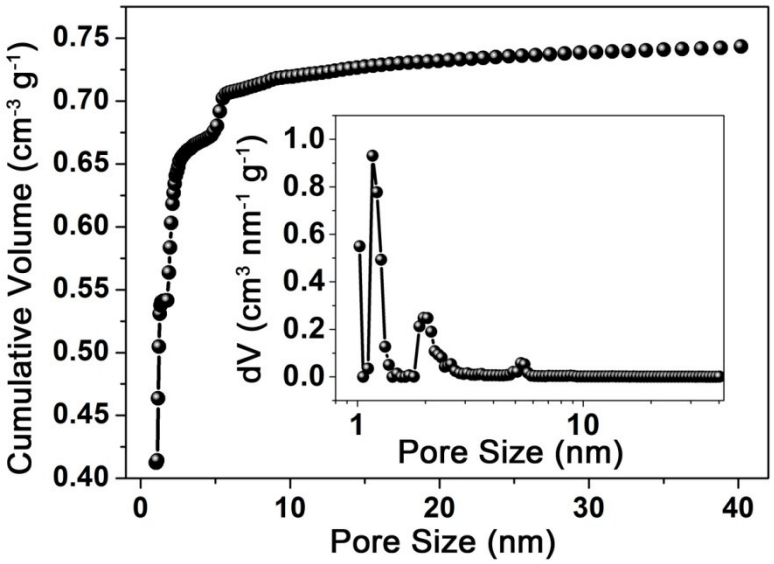

Fig. S19 Cumulative pore volume (pore-size distribution inset) for Kuraray YP-50 (calculated by using a slit/cylindrical NLDFT model).

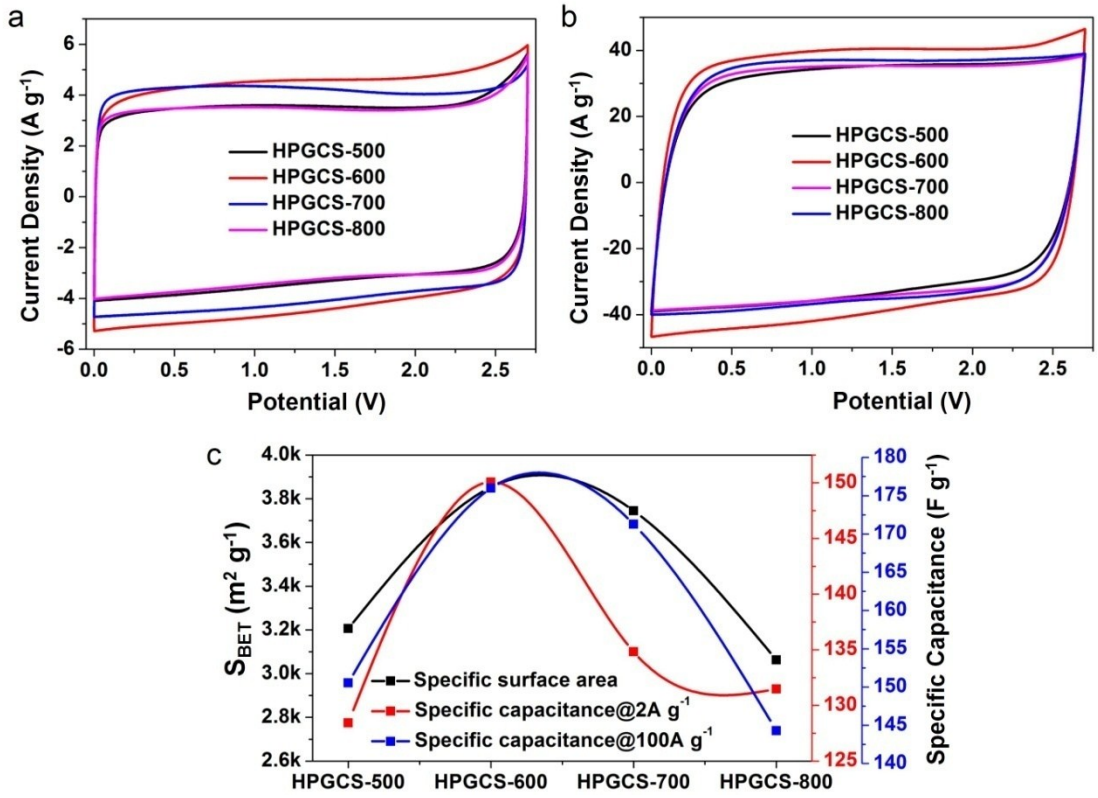

Fig. S20 The electrochemical performance of HPGCS-x (500, 600, 700, 800). (a) the cyclic voltammetry curves at a scan rate of 50 mV s^{-1}, (b) the cyclic voltammetry curves at a scan rate of 500 mV s^{-1}, (c) the specific capacitance with a current density of both 2 A g^{-1} and 100 A g^{-1} versus the specific surface area.

As shown in Fig. 18a, the cyclic voltammetry curves for all HPGCS-x (500, 600, 700, 800) exhibit nearly symmetrical rectangular shape from 0 to 2.7 V at a scan rate of 50 mV s^{-1}. With the elevated scan rate to 500 mV s^{-1}, the cyclic voltammetry curves for all HPGCS-x (500, 600, 700, 800) also show rectangular shap (Fig. 18b), indicating the outstanding capability of carbon materials to transport ions and to conduct electrons. Due to the pore structure is similar, the rate performance of all HPGCS-x (500, 600, 700, 800) are close. As shown in Fig. 18c, the specific capacitance with a current density of both 2 A g^{-1} and 100 A g^{-1} are positive correlation with specfic surface area of HPGCS-x (500, 600, 700, 800).

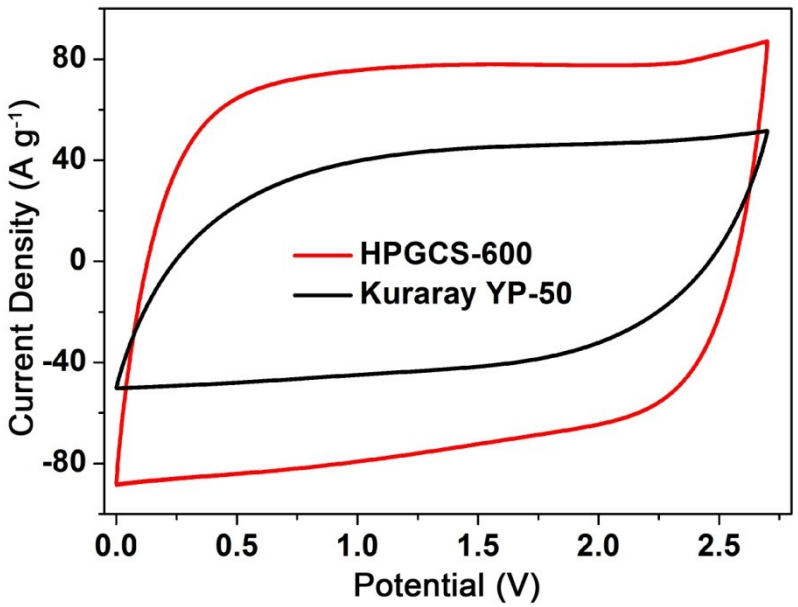

Fig. S21 The CV curves of supercapacitors based on HPGCS and Kuraray YP-50 at a scan rate of 100 mV s^{-1}.

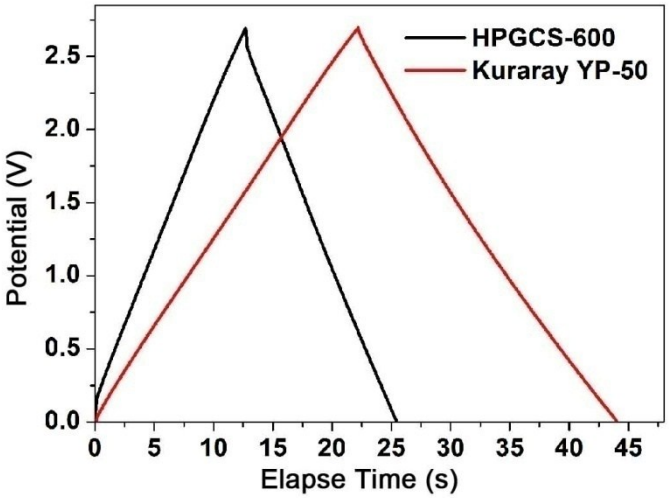

Fig. S22 Typical galvanostatic charge/discharge curves of supercapacitors based on HPG carbon electrode at current density of 10 A g^{-1}.

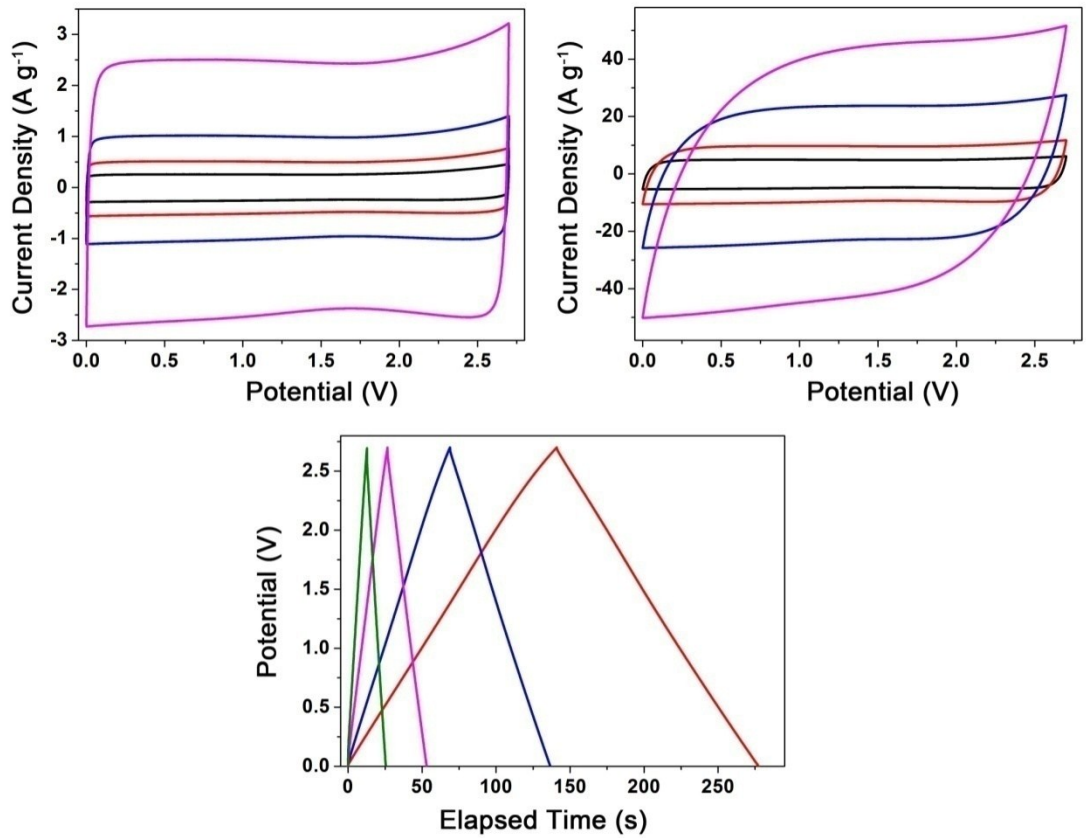

Fig. S23 The CV curves of supercapacitors based on HPGCS at scan rate range from 2 to 1000 mV s^{-1}. Typical galvanostatic charge/discharge curves of supercapacitors based on HPGCS electrode at current density of 1, 2, 5, 10 A g^{-1}.

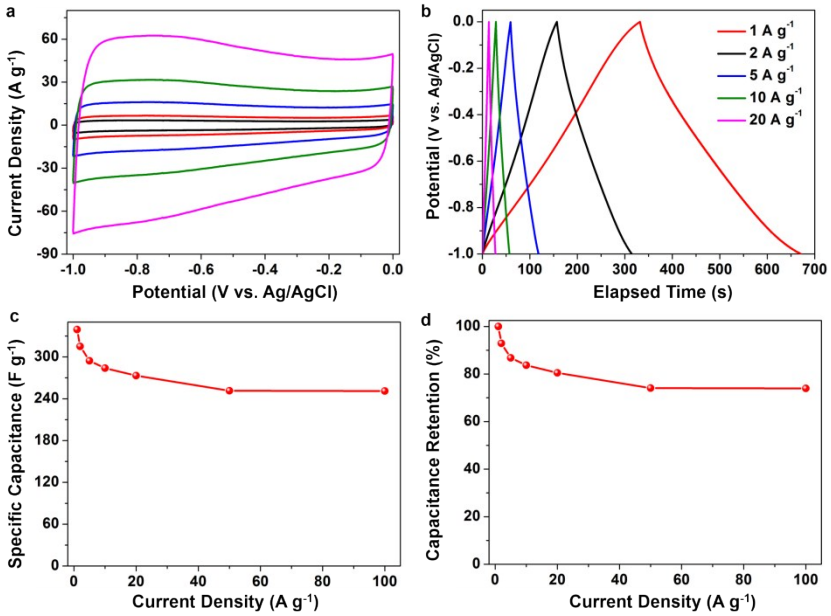

Fig. S24 The electrochemical performance of HPGCS-600 with a three-electrode configuration in 6M KOH aqueous electrolyte. (a) Cyclic voltammetry curves with varied scan rates. (b) Typical galvanostatic charge/discharge curves at current density of 1, 2, 5, 10, 20 A g^{-1}. (c, d) The rate performance curves.

We also studied the electrochemistry performance of HPGCS in 6M KOH solution. As shown in Fig. S22a, the cyclic voltammetry curves of HPGCS-600 show rectangular curves over a wide range of voltage scan rates (from 10 to 200 mV s^{-1}), indicating the outstanding capability of carbon materials to transport ions and to conduct electrons. The typical galvanostatic charge/discharge profiles with ideal triangle wave shape at different current densities are shown in Fig. S22b. The specific capacitance was calculated from the discharge curves with values of 339 F g^{-1} obtained at current densities of 1 A g^{-1}. The HPGCS-600 showed a capacitance of 251 F g^{-1} at a current density of 100 A g^{-1}, corresponding to a capacitance retention of 74% (as shown in Fig. S22c, d). The HPGCS-600 with high SSA and 3D hierarchical porous structures also endow HPGCS-600 with high specific capacitance and excellent rate performance in acqueous electrolyte, outperforming most reported carbon nanomaterials.

Table S1 Elemental analysis of MS-x.

Sample	C (at.%)	O (at.%)	N (at.%)	P (at.%)
MS-500	27.84	37.84	15.13	19.19
MS-600	33.05	29.18	16.28	21.49
MS-700	35.42	27.94	16.02	20.62
MS-800	34.65	23.84	20.17	21.34

Table S2 The comparison of I_D/I_G with the reported porous carbon materials for supercapacitors.

Materials	I_D/I_G	Temperature (°C)	Catalyst	Reference
Porous graphitic carbon	0.92-1.82	800	Fe	*Scientific Reports* 2013, **3,** 2477
Banana peels-derived carbon	1.00	850	No	*Electrochimica Acta* 2018, **262**, 187
Miscanthus-derived carbon	2.97-4.53	900	No	*ACS Sustainable Chemistry & Engineering* 2018, **6**, 318
a-MEGO	1.19	800	No	*Science* 2011, **332**, 1537
Porous carbon foams	1.99	800	No	*Nano Research* 2016, **9**, 2875
Activated graphene	1.11	850	No	*Journal of Materials Chemistry A* 2015, **3**, 9543
Rice husk -derived carbon	1.07	850	No	*Electrochimica Acta* 2016, **192**, 110
Porous carbon nanosheets	1.08	800	No	*Chemistry of Materials* 2014, **26**, 6896
Hierarchical carbon	1	900	No	*Advanced Materials* 2016, **28**, 5222
Human hair-derived carbon	1.10-1.46	700-900	No	*Energy & Environmental Science* 2014, **7**, 379
Prolifera green tide-derived carbon	1.13	900	No	*Advanced Functional Materials* 2016, **26**, 8487
Carbon nanosheets	1.08	800	No	*ACS Nano* 2013, **7**, 5131

Table S3. The summary of the detailed SSA and pores of HPGCS

Sample	S_{BET} ($m^2\ g^{-1}$)	V_{TOTAL} ($cm^3\ g^{-1}$)	V_{MICRO} ($cm^3\ g^{-1}$)	S_{MICRO} ($m^2\ g^{-1}$)
HPGCS-500	3206	2.308	0.807	1679
HPGCS-600	3853	2.788	1.067	2332
HPGCS-700	3745	2.495	0.878	1876
HPGCS-800	3063	2.392	0.494	1085
YP-50	1681	0.793	0.618	1526

Table S4. The summary of the specific capacitance reported in recent literature.

Sample	S_{BET} (m^2 g^{-1})	Electrolyte	Current Density (A g^{-1})	Specific Capacitance (F g^{-1})	Ref
a-MEGO	3100	$TEABF_4$/AN	0.1	150	[3]
	2400	$BMIMBF_4$/AN	1.4	165	
aG-O14 film	2400	$TEABF_4$/AN	10	120	[4]
SG	710	$TEABF_4$/AN	1	190	[5]
			100	58	
PCNS-6	1947	$TEABF_4$/AN	0.25	173	[6]
			10	76	
HMC-800	1306	$LiPF_6$/EC–DEC	2	107	[7]
aPG-10	2582	$BMIMPF_6$/AN	2	163	[8]
		$TEABF_4$/AN	1	126	
SHSG-8	709	$EMIMBF_4$/AN	2	172	[9]
			100	125	
A-aMEGO	3100	$BMIMBF_4$/AN	1	137	[10]
asMEG-O	3290	$BMIMBF_4$ /AN	2.1	167	[11]
AHPC	3270	$TEABF_4$/AN	1	186	[12]
			10	168	
HPNC-NS	2494	$EMIMBF_4$/AN	10	155	[13]
Hurd-a-3	2879	$TEABF_4$/AN	1	144	[14]
			10	121	
HPC-950	1831	Et_4NBF_4/AN	0.1	127	[15]
GNa-CA	1890	$TEABF_4$/AN	0.1	135	[16]

RBC-4	2475	$EMIMBF_4$/AN	0.1	196	[17]
			10	133	
Neem leaf derived carbon	1230	$LiPF_6$/EC–DEC	2	88	[18]
CK-850	2220	$TEABF_4$/AN	5	134	[19]

Reference

[1] J. Zhang, L. Qu, G. Shi, J. Liu, J. Chen, L. Dai, Angew. Chem. Int. Ed. **2016**, 55, 2230.

[2] G. Wu, N. H. Mack, W. Gao, S. Ma, R. Zhong, J. Han, J. K. Baldwin, P. Zelenay, ACS Nano **2012**, 6, 9764.

[3] Y. Zhu, S. Murali, M. D. Stoller, K. J. Ganesh, W. Cai, P. J. Ferreira, A. Pirkle, R. M. Wallace, K. A. Cychosz, M. Thommes, D. Su, E. A. Stach, R. S. Ruoff, Science **2011**, 332, 1537.

[4] L. L. Zhang, X. Zhao, M. D. Stoller, Y. Zhu, H. Ji, S. Murali, Y. Wu, S. Perales, B. Clevenger, R. S. Ruoff, Nano Lett. **2012**, 12, 1806.

[5] X.-F. Jiang, X.-B. Wang, P. Dai, X. Li, Q. Weng, X. Wang, D.-M. Tang, J. Tang, Y. Bando, D. Golberg, Nano Energy **2015**, 16, 81.

[6] C. Chen, D. Yu, G. Zhao, B. Du, W. Tang, L. Sun, Y. Sun, F. Besenbacher, M. Yu, Nano Energy **2016**, 27, 377.

[7] W. Qian, F. Sun, Y. Xu, L. Qiu, C. Liu, S. Wang, F. Yan, Energy & Environmental Science **2014**, 7, 379.

[8] J. Xu, Z. Tan, W. Zeng, G. Chen, S. Wu, Y. Zhao, K. Ni, Z. Tao, M. Ikram, H. Ji, Y. Zhu, Adv. Mater. **2016**, 28, 5222.

[9] C. Li, X. Zhang, K. Wang, X. Sun, G. Liu, J. Li, H. Tian, J. Li, Y. Ma, Adv. Mater. **2016**, 1604690.

[10] M. Ghaffari, Y. Zhou, H. Xu, M. Lin, T. Y. Kim, R. S. Ruoff, Q. M. Zhang, Adv. Mater. **2013**, 25, 4879.

[11] T. Kim, G. Jung, S. Yoo, K. S. Suh, R. S. Ruoff, ACS Nano **2013**, 7, 6899.

[12] D. Kang, Q. Liu, J. Gu, Y. Su, W. Zhang, D. Zhang, ACS nano **2015**, 9, 11225.

[13] J. Hou, C. Cao, F. Idrees, X. Ma, ACS Nano **2015**, 9, 2556.

[14] W. Sun, S. M. Lipka, C. Swartz, D. Williams, F. Yang, Carbon **2016**, 103, 181.

[15] H. Wang, S. Yu, B. Xu, Chem. Commun. **2016**, 52, 11512.

[16] A. B. Fuertes, M. Sevilla, ACS Applied Materials & Interfaces **2015**, 7, 4344.

[17] J. Hou, C. Cao, X. Ma, F. Idrees, B. Xu, X. Hao, W. Lin, Sci. Rep. **2014**, 4, 7260.

[18] M. Biswal, A. Banerjee, M. Deo, S. Ogale, Energy & Environmental Science **2013**, 6, 1249.

[19] M. Sevilla, A. B. Fuertes, ACS Nano **2014**, 8, 5069.